Biochimica et Biophysica Acta 1838 (2014) 2149–2159

Contents lists available at ScienceDirect

Biochimica et Biophysica Acta

journal homepage: www.elsevier.com/locate/bbamem

Implicit membrane treatment of buried charged groups: Application to peptide translocation across lipid bilayers ☆

Themis Lazaridis *, John M. Leveritt III, Leo PeBenito

Department of Chemistry, City College of New York, 160 Convent Avenue, New York, NY 10031, USA

ARTICLE INFO

Article history:
Received 13 December 2013
Accepted 10 January 2014
Available online 10 February 2014

Keywords:
Lipid bilayer
Implicit solvent
Molecular dynamics simulations
Voltage sensor
Cell penetrating peptides
Arginine

ABSTRACT

The energetic cost of burying charged groups in the hydrophobic core of lipid bilayers has been controversial, with simulations giving higher estimates than certain experiments. Implicit membrane approaches are usually deemed too simplistic for this problem. Here we challenge this view. The free energy of transfer of amino acid side chains from water to the membrane center predicted by IMM1 is reasonably close to all-atom free energy calculations. The shape of the free energy profile, however, for the charged side chains needs to be modified to reflect the all-atom simulation findings (IMM1-LF). Membrane thinning is treated by combining simulations at different membrane widths with an estimate of membrane deformation free energy from elasticity theory. This approach is first tested on the voltage sensor and the isolated S4 helix of potassium channels. The voltage sensor is stably inserted in a transmembrane orientation for both the original and the modified model. The transmembrane orientation of the isolated S4 helix is unstable in the original model, but a stable local minimum in IMM1-LF, slightly higher in energy than the interfacial orientation. Peptide translocation is addressed by mapping the effective energy of the peptide as a function of vertical position and tilt angle, which allows identification of minimum energy pathways and transition states. The barriers computed for the S4 helix and other experimentally studied peptides are low enough for an observable rate. Thus, computational results and experimental studies on the membrane burial of peptide charged groups appear to be consistent. This article is part of a Special Issue entitled: Interfacially Active Peptides and Proteins. Guest Editors: William C. Wimley and Kalina Hristova.

1. Introduction

The main function of cell membranes is to prevent the uncontrolled exchange of highly polar species, especially ions, between the cell and its environment. This is accomplished by the high cost of partitioning such species from water into the nonpolar membrane interior [1,2]. The energy barrier is highest for nontitratable charges, such as small ions. Titratable groups, such as the ionizable protein side chains, face a lower barrier because they can pick up or lose a proton and become neutral. However, the cost is still substantial, of the order 10–20 kcal/mol. This conventional view has been challenged in recent years by a number of observations: relatively facile transmembrane (TM) insertion of highly charged helices by the translocon [3], modest destabilization of the membrane protein OmpLA by insertion of charged side chains in the middle of the membrane [4], and the apparent ability of many positively charged peptides to cross cell membranes [5].

Valuable information has been obtained by all-atom molecular dynamics simulations. For example, it has repeatedly been observed that insertion of charged groups in the nonpolar membrane interior generates "water defects" which apparently reduce the free energy cost of partitioning [6–10]. A simulation of the S4 helix of the potassium channel voltage sensor showed how the membrane can deform to accommodate the charged groups [11]. The free energy cost of these deformations is more difficult to evaluate, but free energies for translocation of charged groups have been obtained by all-atom calculations [9,10,12]. The resulting values were significantly lower than what one would expect from continuum electrostatics, but much higher than the values inferred from the experiments mentioned above [4,13]. Careful analysis of the data and the experiments have come a long way toward reconciling these conflicting observations [14–18] but some discrepancy still persists [19].

All-atom simulations are highly informative but very costly, prohibitively so for some applications. Implicit membrane models, which attempt to take into account the lipid and water effects through a solvation free energy term in the energy function, offer many advantages, such as speed, rapid equilibration, and easy interpretation. However, they are usually deemed too simplistic to deal with issues such as the burial of charged groups. Two major difficulties are the inability of the membrane to deform and the "water defects". Most implicit membrane models consider the membrane as fixed, although attempts to relax this assumption have been reported [20–22].

☆ This article is part of a Special Issue entitled: Interfacially Active Peptides and Proteins. Guest Editors: William C. Wimley and Kalina Hristova.

* Corresponding author. Tel.: +1 212 650 8364.
E-mail address: tlazaridis@ccny.cuny.edu (T. Lazaridis).

0005-2736/$ – see front matter © 2014 Elsevier B.V. All rights reserved.
http://dx.doi.org/10.1016/j.bbamem.2014.01.015

Here we consider the possibility of taking into account both of the above effects, in an approximate way, in the context of the implicit membrane model IMM1. Thinning is treated by performing simulations at different membrane thicknesses and adding a membrane deformation free energy estimated from an elasticity theory of lipid membranes. Water defects are implicitly accounted for by changing the shape of the free energy profile, as suggested by all-atom simulations. The model is validated by comparison to transfer energies obtained by all-atom simulations [10,12] and experimental pKa data [23] and tested on the voltage sensor of voltage-gated potassium channels and its isolated S4 helix.

With this new model we begin to address the problem of peptide translocation across bilayers, a topic of great fundamental and practical interest due to its potential impact on drug delivery methods [24]. Several all-atom studies have already been performed. Garcia and coworkers saw pore formation and translocation at high concentration of the HIV Tat peptide [25]. This study was criticized for lack of counterions by other authors, who computed a free energy barrier of 18 kcal/mol for penetratin and 36 kcal/mol for HIV Tat [26]. A barrier of 29 kcal/mol was calculated for a cyclic R9 [27]. Another study of transportan found a 16 kcal/mol barrier for translocation, but also an excessively large (−72 kcal/mol) free energy of adsorption to the membrane interface [28].

Two mechanisms are currently envisioned for peptide translocation. In the first, several peptides come together and facilitate the opening of an aqueous pore in the membrane. When this transient pore closes, some peptides end up on the other side of the bilayer [29]. This mechanism is expected to be accompanied by some leakage of vesicle contents. The second mechanism involves direct translocation of monomeric peptide through the membrane without pore formation, in which case leakage is expected to be minimal. Recent experimental work has provided intriguing new data and helped clarify the difference between the two mechanisms [30–32]. Wimley and coworkers screen for peptides that translocate without leakage [30,31]. Almeida and coworkers in recent work with giant vesicles follow both peptide translocation and dye leakage. In most of their experiments translocation is accompanied by leakage, although they do occasionally observe translocation without leakage [32].

In this work we focus on peptide translocation by the second mechanism, monomeric peptide diffusion without pore formation. Assuming a helical secondary structure, we create a map of the effective energy as a function of position and tilt and on this map we identify minimum energy pathways and transition states. From the magnitude of the barriers we estimate the time scale of translocation. We apply this approach to peptides studied recently by the Wimley and Almeida groups and obtain results consistent with their findings.

2. Methods

2.1. IMM1

The implicit membrane model IMM1 [33] is an extension of the EEF1 model for water-soluble proteins [34]. EEF1 uses the extended atom CHARMM force field (param19) [35] with neutralized ionic side chains and a linear distance dependent dielectric constant ($\varepsilon = r$) for the electrostatic interactions. IMM1 extends EEF1 to heterogeneous membrane-water systems by allowing the solvation parameters to vary between values corresponding to aqueous solution and values corresponding to cyclohexane. A sigmoidal function is used to switch from one region to the other:

$$f(z') = \frac{z'^n}{1 + z'^n} \tag{1}$$

where $z' = |z| / (T/2)$, z is the position along the membrane normal, and T is the thickness of the nonpolar membrane core. The parameter n controls the steepness of the transition. The exponent $n = 10$ gives a region of 6 Å over which the environment transitions from 90% nonpolar to 90% polar. To account for the strengthening of electrostatic interactions in the membrane, a modified dielectric screening function is used

$$\varepsilon = r^{f_{ij}} \quad f_{ij} = \alpha + (1-\alpha)\sqrt{f_i f_j}. \tag{2}$$

The value 0.85 for the adjustable parameter α was found to give membrane binding energies in accord with experiment. Unless otherwise stated, the width of the lipid membrane was 26 Å in all simulations reported in this work. No surface charge was included [36]; therefore the calculations pertain to zwitterionic membranes.

2.2. IMM1 with linear switching function for charged side chains (IMM1-LF)

While the magnitude of the barrier is similar in IMM1 and explicit simulation free energy profiles (see Section 3), the shape of the profile is not. IMM1 uses a relatively abrupt sigmoidal switching function to describe the transition between nonpolar and polar regions. The explicit free energy profiles have a similar shape for the polar amino acid side chains, but a triangular, "Λ" shape for the charged ones [9,14,37,38]. As a result, IMM1 provides a good estimate at the center of the membrane but overestimates the free energy at other points (see Fig. 1). A simple fix for this is to use a linear switching function ($f = |z'|$ for $|z'| < 1$ and $f = 1$ for $|z'| \geq 1$) for the charged side chains. We refer to this model as IMM1-LF, LF meaning "linear f".

Another important observation is that as the membrane becomes thinner, the barrier at the center is reduced leaving the slope of the Λ nearly the same [39]. The simplest way to reproduce this in IMM1 is to adjust the CHEX solvation parameters so as to obtain the desired slope of the free energy profile, i.e. $(G_{wat} - G_{hex}) / 26\ Å = (G_{wat} - G_{hex}') / T$. However, in calculations in thinner membranes to estimate optimal membrane deformations (see below), it is best to leave the parameters unchanged, because deformation effects are already included in the explicit simulation profiles.

2.3. Membrane thinning

Although the membrane is usually fixed in implicit membrane models, there is a way to account for local deformations. One first performs calculations for a range of membrane thicknesses (T) to compute the effective energy W as a function of T. An estimate of the membrane deformation free energy ΔG^{def} as a function of T is then added to the resulting energies and the thickness that minimizes the sum of W and

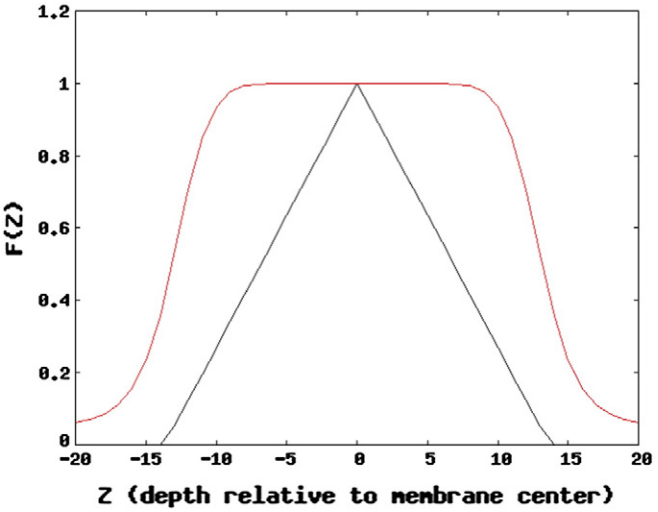

Fig. 1. Sigmoidal (red) vs. linear (black) switching function.

ΔG^{def} is selected as the optimal result [40]. As in previous work [41], we use the spring model proposed by Andersen and coworkers [42] to estimate the membrane deformation free energy. According to this model, the deformation free energy can be calculated as $\Delta G^{def} = H(\Delta T)^2$, where ΔT stands for the deformation of the membrane and H is the spring constant that can be determined using the equation:

$$H = H^* \left(\frac{K_a}{K_a^*}\right)^{\nu} \left(\frac{K_c}{K_c^*}\right)^{\mu}. \quad (3)$$

In Eq. 3, K_a^*, K_c^* and H^* are the reference values for the expansion modulus (K_a), the splay-distortion modulus (K_c) and the spring constant (H), respectively with values: $K_a^* = 142.5$ pN/nm, $K_a = 254$ pN/nm, $K_c^* = 28.5$ pN · nm, $K_c = 76$ pN · nm, $\nu = 0.667$ and $\mu = 0.334$ [43]. The parameter H^* is related to the radius r (in nm) of the inserted cylinder that causes the deformation according to the relation:

$$H^* = 15.2 \cdot \left(\frac{r}{1.0}\right)^{0.815} \quad \text{kcal/mol}. \quad (4)$$

For a single helix, the radius is about 0.5 nm and one obtains $\Delta G^{def} = 17.6\ (\Delta T)^2$ kcal/mol, which gives $\Delta G^{def} = 0.7, 2.8, 6.3, 11.3, 17.6$ kcal/mol for $\Delta T = 2, 4, 6, 8, 10$ Å, respectively.

2.4. Transfer energies of side chain analogs

Models for the side chain analogs were created by truncating the corresponding side chain at the C^{β}, which was changed from CH2E to CH3E atom type. Initial coordinates were created using Maestro (Schrodinger, Inc). The molecules were initially oriented with their principal axis along the x-axis. A constraint was applied to keep the molecules near the center of the membrane and MD simulations were run for 1 ns with IMM1, followed by energy minimization. The final minimized energy is taken to be the energy of the analog in the membrane. A second simulation for each analog was run in water with EEF1 using the same protocol (without the constraint). The transfer energy is the difference between the energies in solution and in the membrane. Using the average energy over the dynamics or the initial energy without minimization gives essentially identical results.

2.5. GWALP23 peptides

We studied eight variants of the GWALP23 peptide [23] with sequence acetyl-GGAL[W/Y](LA)$_6$LWLAGA-NH$_2$ with R or K replacing a Leu at position 12 or 14. Each peptide was generated as an ideal helix and placed in TM orientation. After an initial 100-ps simulation and energy minimization, a 5-ns MD simulation was run with a 2-fs time step, saving the coordinates every 100 steps. For each frame in the trajectory the energy difference between the TM structure and the same structure in water was calculated. The average of these energy differences over the trajectory is an estimate of the binding energy. pKa values were computed using the standard thermodynamic cycle whose vertical steps involve insertion of the protonated and deprotonated analogs into the membrane and the horizontal steps are deprotonation in solution and in the membrane [12,37]:

$$pKa = pKa_{bulk} + \frac{\Delta G_T}{2.303RT}$$

$$\Delta G_T = \Delta G_2 - \Delta G_1$$

$$\Delta G_1 = \Delta G^{\text{protonated}}_{\text{membrane}} - \Delta G^{\text{protonated}}_{\text{solution}}$$

$$\Delta G_2 = \Delta G^{\text{deprotonated}}_{\text{membrane}} - \Delta G^{\text{deprotonated}}_{\text{solution}}$$

We approximate the free energy of insertion by the effective energy of insertion. The reference pKa values used for solution are 4.0, 4.4, 10.4, 12.0, 7.5, and 3.8 for Asp, Glu, Lys, Arg, N terminus, and C terminus, respectively [44]. The cost of neutralization at pH 7 and 25 °C is 4.1, 3.5, 4.6, 6.8, 0.7, and 4.3 kcal/mol, respectively.

2.6. Voltage sensor and S4 helix

The crystal structure of the voltage sensor of the KvAP potassium channel (pdb id: 1ORS) was used as the starting structure. The molecule was aligned with its principal axis along the membrane normal and subjected to energy minimization and a 1-ns MD simulation in standard IMM1 and IMM1-LF. These MD simulations used the standard Verlet integrator, SHAKE [45] to constrain the bonds involving hydrogen, and a 2-fs time step.

The N-terminal part of the S4 helix (sequence LGLFRLVRLLRFLRILLIIC) was built as an ideal helix and placed in a TM orientation. Energy minimization was followed by MD simulation, typically of 1 ns duration. The Nose–Hoover thermostat was used to maintain the temperature at 300 K. Average effective energies were calculated over the last 0.6 ns. Error bars were estimated as the standard deviation of the averages over four portions of the last 0.6 ns of the trajectory.

2.7. Translocation pathways

The average effective energy <W> as a function of z (the position of the center of mass along the membrane normal) and tilt angle θ (the angle between the N-C vector and the positive z axis) was calculated as follows. The MMFP facility in CHARMM was used to constrain the center of mass at given values of z and the HELIX constraint facility [46] was used to constrain the tilt angle. A regular grid of points for z (0 to 26 Å at 3.25 Å interval) and θ (0 to 180° at 30° interval) was scanned. The negative z values were filled by using the symmetry relationship $W(z,\theta) = W(-z,\pi-\theta)$. Because the high energies sampled at certain points were found to distort the helix and create problems with the helix tilt constraint, NOE constraints between i and i + 4 backbone atoms were used to maintain the helical structure. The use of these constraints may affect somewhat the energy values and the positions of the local minima on the energy surface compared to unconstrained simulations. At each grid point a 100-ps MD simulation was run and the average effective energy was calculated over the last 50 ps. Contour plots of the average effective energy as a function of z and θ were generated using the program R [47]. This approach is applied to the S4 helix, two peptides studied by Marks et al. [30], TP2 (PLIYLRLLRGQF) and ONEG (PLGRPQLRRGQF), and two peptides studied by Wheaten et al. [32], TP10W (AGWLLGKINLKALAALAKKIL-amide) and DL1 (acetyl-MAQKIISTIGKLVKWIIKTVNKFTKK, experiment uses formyl instead of acetyl).

3. Results

3.1. Transfer energies predicted by IMM1

In EEF1 [34] the charged groups of titratable residues were given a zero net charge and their solvation parameters were reduced to about −20 kcal/mol. These solvation parameters were largely arbitrary; the only requirement was that the combination of partial charge distribution and solvation parameters gave a reasonable interaction energy of exposed salt bridges. Small adjustments were made later based on calculated potentials of mean force in water [48]. For the membrane interior in IMM1 these charged groups were given solvation parameters pertaining to the corresponding neutral group in nonpolar solvents.

The transfer of a charged group from water to the membrane interior is governed by the difference in these solvation parameters. Neutralized forms of these residues were also created, with solvation parameters pertaining to polar groups. All solvation parameters were extracted from a group contribution analysis of solvation free energy data in cyclohexane.

A few years ago MacCallum and Tieleman (M&T) computed Potentials of Mean Force for small-molecule analogs of 19 amino acid side chains containing all atoms from the C^{β} and beyond [10,12]. Explicit simulation results are not a gold standard, because they can be affected by force field [49] and sampling [50] inadequacies. However, in the absence of experimental data for bilayers they provide a most useful benchmark. We computed transfer energies for the same analogs to compare with M&T's results (Table 1). The correlation coefficient between the two scales is 0.95. The IMM1 parameters were derived from an additive group-contribution analysis of cyclohexane data [51], which are sometimes closer to IMM1 and other times closer to the explicit results. Surprisingly, even the IMM1 values for the charged groups are not far from the atomistic results. This is clearly fortuitous, given the way these parameters were derived, as described above. Table 1 also includes data for methyl-guanidinium and methyl-ammonium, recently studied by the Allen group [52]. Again, the comparison is quite favorable.

Some quantitative discrepancies do exist between the two scales. For example, the transfer free energy is underestimated for charged acidic groups and overestimated for the protonated acidic groups. In IMM1 and experiment, burial of Glu is less unfavorable than that of Asp, as one would expect from the additional CH_2 group. Unexpectedly, the opposite is seen in the explicit simulations. For the basic groups the IMM1 numbers are higher than the M&T values, except for neutral Lys. The comparison with the Li et al. values is similar, except for methylammonium for which Li et al. obtain a relatively high value.

Table 1
Transfer effective energies (kcal/mol) from water to the membrane center computed by IMM1 and compared to the explicit all-atom results of MacCallum and Tieleman [10,12] or Li & Allen in DPPC [52] and experimental results of Radzicka & Wolfenden [51]. The values for the titratable residues were read off Fig. 5 of Ref [12]. The (pH 7) entries give the true barrier allowing titration, i.e. the lower of two values: that for the charged species or that for the neutral species ±2.3RT(pKa-pH).

AA	IMM1	M&T	R&W
Leu	−5.7	−3.6	−4.92
Ile	−5.5	−5.3	−4.92
Val	−4.6	−3.3	−4.04
Ala	−1.8	−2.0	−1.81
Phe	−4.1	−3.1	−2.98
Trp	−0.6	−1.2	−2.33
Cys	−1.6	−0.8	−1.28
Met	−2.9	−1.1	−2.35
Tyr	0.5	1.6	0.14
Ser	3.2	3.8	3.40
Thr	2.1	3.3	2.57
Asn	5.8	5.7	6.64
Gln	4.2	4.8	5.54
Asp	16.5	19.0	
Glu	14.7	20.3	
Lys	13.4	11.7	
Arg	18.3	13.9	
Asp0	6.9	2.4	
Glu0	5.4	4.3	
Lys0	−0.8	0.5	
Arg0	8.2	6.2	
Asp(pH 7)	11.0	6.5	8.72
Glu(pH 7)	8.9	7.8	6.81
Lys(pH 7)	3.8	5.1	5.55
Arg(pH 7)	15.0	13.0	14.92
		Li & Allen	
Methyl-ammonium	17.1	22.3	
Methyl-guanidinium	21.4	20.0	
Methyl-amine	2.6	2.3	
Methyl-guanidine	10.6	7.3	

The IMM1 transfer values of the neutral and charged groups are such that we predict all titratable analogs to be neutral at the membrane center (i.e. ΔW(neutral) ± 2.3RT(pH-pKa) < ΔW(charged)). This is in agreement with the explicit results, except for Arg, for which equal probability was found for the neutral and charged forms. The other polar side chains compare quite favorably. Some discrepancies are observed in the nonpolar transfer energies. IMM1 and experiment gives equal transfer energies for Leu and Ile, but M&T find a smaller value for Leu. The transfer of S-containing analogs is more favorable in IMM1 and experiment than the explicit results. These comparisons suggest that a slight adjustment of the solvation parameters in IMM1 could improve agreement with experiment and/or explicit simulation. Nevertheless, here we will use the original parameters and leave any adjustments for future work.

To include the effects of the peptide backbone we also performed a "host-guest" study placing each amino acid at the center of a transmembrane polyalanine helix or beta strand. The whole-residue transfer energies we obtain are higher than those of the side chains by roughly 2 kcal/mol for the helix and 4 kcal/mol for the beta strand. Thus, the formation of a backbone hydrogen bond in the membrane interior lowers the energy by about 2 kcal/mol. For the burial of blocked helical ends into the membrane IMM1 predicts a cost of about 5 kcal/mol for the N terminal end and 11 kcal/mol for the C terminal end. These values are quite close to explicit simulation estimates [53].

3.2. Comparison with experimental pKa values

Several simulation studies examined whether arginine is protonated or neutral at the membrane center and found that Arg remains mostly protonated up to the center of the membrane [37,54,55], or that it has about equal probability to be protonated or deprotonated at the membrane center [10,12]. The pKa shift, however, does depend on the lipid composition [56]. Koeppe and coworkers recently reported experimental pKa values or limits thereof in variants of the GWALP23 model peptide [23]. They found that Lys inserted in the bilayer interior has a pKa below 7 but Arg remains protonated at pH values up to 9. Data like these can be used to benchmark our treatment for the charged groups.

We computed pKa shifts in the GWALP23 peptide using a standard thermodynamic cycle (see Section 2). Table 2 reports pKa values obtained for the system studied by Gleason et al. using the standard IMM1 and IMM1-LF, in which the a linear switching function is used for the charged groups (see Section 2). As can be seen in Table 2, all peptides are favorably inserted in the membrane but the energy of insertion is highly dependent on sequence. With standard IMM1, the pKa values of arginine remain higher than those of lysine within the membrane, but the pKa shifts are quite large, so that all the charged side chains would be neutral in the membrane at neutral pH. This is not in agreement with experiment [23]. In proteins, pKa values for buried Lysine range from 5.3 to 9.3 [57]. Here, they are between 1 and 4, whereas a value of 6.2 to 6.8, depending on temperature, has been determined

Table 2
pKa values for GWALP23 analogs [23] using standard IMM1 and IMM1-LF. ΔW is the effective energy of transferring the peptide from the membrane to water. The statistical uncertainty on pKa is up to 0.3 units.

	IMM1			IMM1-LF		
	ΔW_{cha}	ΔW_{neu}	pKa	ΔW_{cha}	ΔW_{neu}	pKa
GWAL($_6$)PW5K12	7.2	18.8	2.0	11.2	20.5	3.7
GWAL($_6$)PW5K14	6.8	19.5	1.2	14.9	20.8	6.1
GWAL($_6$)PW5R12	4.6	13.3	5.6	11.4	15.9	8.7
GWAL($_6$)PW5R14	2.4	13.7	3.8	13.6	14.5	11.4
GWAL($_6$)PY5K12	9.8	18.4	4.2	14.6	21.4	5.5
GWAL($_6$)PY5K14	7.4	20.4	0.9	16.2	21.8	6.4
GWAL($_6$)PY5R12	4.8	11.5	7.1	12.9	13.6	11.5
GWAL($_6$)PY5R14	2.9	11.7	5.6	12.7	11.3	13.0

for K14 [23]. Thus, the desolvation of the charged Lys and Arg is overestimated by standard IMM1.

Using IMM1-LF the Arg-containing peptides tilted substantially and buried the (blocked) N-terminus in the membrane. This happens because the cost of burying the blocked N-terminus is slightly smaller than the energy gained by the full exposure of Arg to the aqueous interface. This is not in agreement with the experiment, which finds small tilt angles for at least the R14 peptides. This problem will be explored in more detail in future work. For now, we compute pKa's constraining the peptides to remain transmembrane and report the results in Table 2. Now the pKa shifts are smaller. All lysines have a pKa below 7 and all arginines are above or near the threshold that experiment would have detected. A more precise calibration of the model can be done with additional experimental and computational data.

3.3. Application to a voltage sensor

The voltage sensor of voltage-gated potassium channels has been the focus of intense study. Several crystal structures showed that it is a four-helix bundle [58–61]. While there was initially some uncertainty about its orientation [58], it is now established that it integrates in the membrane with the helices roughly parallel to the membrane normal [61–63]. Several MD simulations showed it to be stable in the membrane on the time scale of 20–50 ns [64–67].

The voltage sensor has two aqueous crevices on the intracellular and extracellular side that give it an hourglass-like shape, so it is not an ideal system for a standard implicit membrane treatment. However, IMM1 predicts stable membrane insertion with a transfer effective energy from water to the membrane of about −40 kcal/mol. The RMSD after 1 ns of MD is about 3.4 Å, somewhat higher than in explicit simulations. This is primarily due to a partial collapse of the extracellular aqueous crevice. The first two Arg of S4 are near the aqueous interface (Fig. 2). These results are similar to what has been observed in all-atom explicit simulations [64–67]. So, despite the obvious limitation with the aqueous crevices, the model reproduces the stable insertion and the overall configuration of the voltage sensor in membranes. IMM1-LF gives a similar RMSD and an even more favorable membrane insertion energy (−58 kcal/mol).

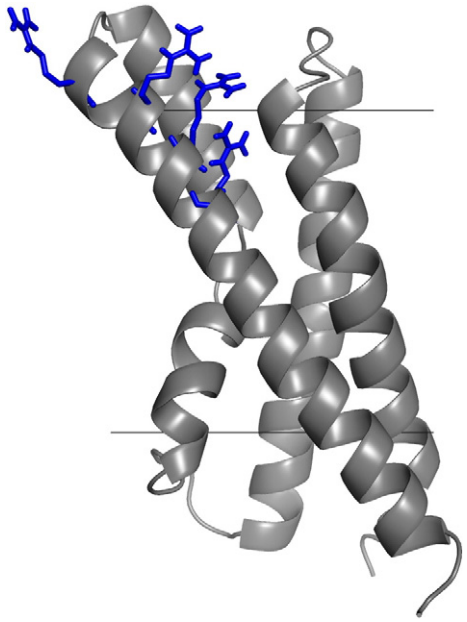

Fig. 2. Structure of the voltage sensor after MD dynamics with IMM1-LF.

3.4. S4 helix insertion

In addition to the intact voltage sensor, several studies focused on the isolated S4 helix, either in its entirety [68] or, more commonly, the N-terminal part, which will also be considered here [3,11,31,69–71]. S4 has been shown to be incorporated in a transmembrane topology by the translocon with a probability that implies a free energy of insertion of only +0.5 kcal/mol [3]. Experiments with vesicles also showed an equilibrium between surface and transmembrane orientations [71]. Solid-state NMR experiments found stable incorporation in the membrane with a 40° tilt angle and 9-Å local membrane thinning [69]. A combination of coarse-grained and all-atom simulations gave a free energy of insertion that seems excessively favorable, −45 kcal/mol [70]. However, earlier experiments indicated an interfacial (INT) orientation for the S4 helix [72,73].

Standard IMM1 predicts interfacial binding of the S4 helix to a neutral membrane (Fig. 3a) with an average effective energy about 9 kcal/mol

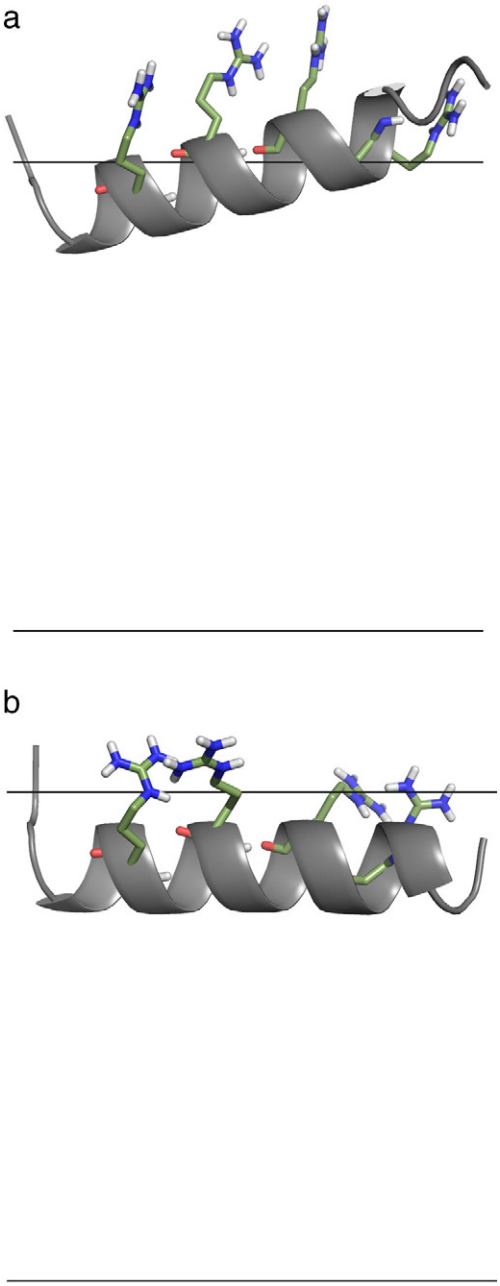

Fig. 3. The interfacial minimum for the S4 helix in a) IMM1 and b) IMM1-LF.

lower than in water. In simulations starting from a TM orientation the peptide moved to an interfacial orientation for T = 24 and 26. For membrane thickness less than 22 Å it stayed TM but there was partial helix unfolding. Constraining the peptide in a TM orientation and consideration of membrane thinning improves the effective energy, but the cost of membrane deformation keeps it more than 10 kcal/mol higher than the interfacial configuration (data not shown).

As expected, IMM1-LF gives a more stable TM configuration. The helix remains well folded (Fig. 4), and the transfer from water into the TM position is now favorable (Table 3). Thinning the membrane does not reduce the energy enough to compensate for membrane deformation. The tilt angle is 31°, comparable with the 40° determined by solid state NMR in a thinner DMPC/DMPG bilayer [69]. The interfacial orientation is now more deeply buried (Fig. 3b) and is also stabilized relative to standard IMM1, but not as much as the TM orientation. As a result, the difference in stability is reduced to about 4 kcal/mol. This result seems reasonable, considering the experimental findings described above.

3.5. S4 helix translocation

It has been shown that the S4 helix is able to translocate through artificial lipid membranes [31], reminiscent of many other cationic peptides, termed cell-penetrating peptides (CPPs), that are able to enter cells and deliver covalently or noncovalently attached cargo [74]. However, classical CPPs like Arg9 were not able to translocate in the assay of Wimley and coworkers [30].

To explore the feasibility of translocation we attempted to calculate translocation pathways and free energy barriers in the following way. To simplify the calculations, the peptide was assumed to translocate as a helix. Two variables were used to map its configuration with respect to the membrane: the position of the center of mass along the bilayer normal (z) and the tilt angle (θ). The rotation angle (describing rotation around the helix axis) was allowed to relax to its optimal value for each pair of z,θ. The desired values of z and θ are enforced using restraints and MD simulations are performed to calculate the average effective energy as a function of z,θ. Optimal pathways, transition states, and effective energy barriers are then determined visually on the W(z,θ) surface. Ideally, one should allow changes in protonation states of all titratable groups at every point on the energy map, but this is not possible to do automatically with our current program and tedious to do manually. Hence, in this preliminary work we use fixed protonation states. Neutralization of Arg does not lead to significant gains (see Table 1), so we treat Arg as charged. Neutralization of the termini or Lys could lower the energy, so we compute maps with charged termini and then examine whether neutralization of the termini at the transition state (TS) would lower the energy.

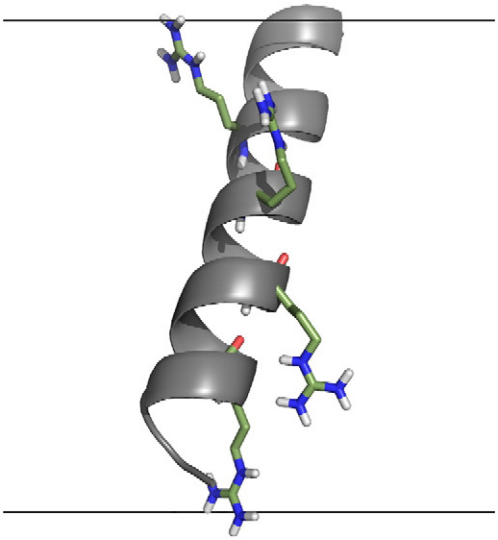

Fig. 4. Transmembrane configuration of the S4 helix after MD with IMM1-LF.

Table 3
Average effective energy of the TM orientation of S4 helix in the IMM1-LF model as a function of membrane thickness.

	<W>	<W> + ΔG^{def}
Water	−361.5 ± 0.5	
Interfacial	−381.7 ± 2.0	
TM T = 26	−377.3 ± 0.7	−377.3 ± 0.7
TM T = 24	−375.5 ± 1.4	−374.8
TM T = 22	−378.1 ± 5	−375.3
TM T = 20	−382.4 ± 1.3	−371.8

The 2-d energy surface for S4 in the original IMM1 (not shown) gives a tilted interfacial configuration as the global minimum. There is no local minimum at the TM configuration and the barrier for translocation is ~45 kcal/mol. The surface obtained with IMM1-LF is shown in Fig. 5. The global minimum is interfacial, parallel to the membrane and the TM configuration is a local minimum. Because of the constraints, the energies are a bit higher than those obtained in the previous section (−377 kcal/mol vs. −382 kcal/mol for INT and −370 kcal/mol vs. −377 for TM). Due to symmetry, there are two equivalent translocation pathways, differing in which terminus goes across first. The transition states, denoted by #, are at about −350 kcal/mol.

To refine the energy of the transition states we performed additional simulations at (8,40) and (5,130), the latter being equivalent to (−5,50). The average energy obtained was −357 kcal/mol for the first barrier and −372 kcal/mol for the second one. They correspond to the configurations shown in Fig. 6, where either the N terminus or the C terminus has just crossed the membrane center. Using the unconstrained INT energy as the reactant state, the first barrier height is about 25 kcal/mol. Because at this barrier the buried N terminus is far from the membrane interface, thinning is unlikely to help reduce this barrier. However, neutralization of the N terminus could. Calculations of the transfer energy for charged and neutral N terminus shows more favorable insertion for the latter by 7 kcal/mol. Subtraction of the neutralization cost (0.7 kcal/mol) leaves a gain of 6.3 kcal/mol. Thus, the refined estimate for the highest barrier becomes 18.7 kcal/mol.

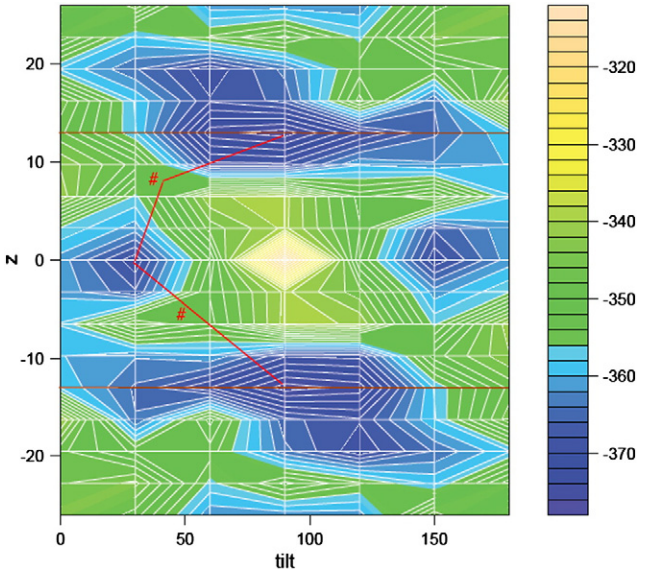

Fig. 5. Effective energy surface for the S4 helix in IMM1-LF. The lines at z = −13, 13 denote the hydrophobic/hydrophilic boundary, the red line denotes the minimum energy pathway, and # the transition states.

3.6. Translocation of Marks–Wimley peptides

In addition to the S4 helix, the Wimley group has used a combinatorial library strategy to generate peptides that spontaneously translocate through lipid membranes [30]. Several sequences containing 2 or 3 arginines were found to have that ability. The arrangement of the arginines appeared to be critical, as certain patterns emerged more frequently than others. The peptides were 12 residues long and seemed to lack secondary structure. No dependence on concentration was detected, suggesting that the peptides translocate as monomers.

In this preliminary study, we chose to focus on one peptide that translocates and one that does not (TP2 and ONEG, respectively) using IMM1-LF. The same peptides have been the subject of CD, neutron diffraction, and leakage studies in zwitterionic membranes [75]. TP2 was found to have higher affinity and insert slightly more deeply in the membrane than ONEG. Both peptides were found to be unstructured in buffer but TP2 attained some beta character upon binding to the membrane. No helix was detected in these experiments. However, we cannot preclude the possibility that the peptides adopt a helical structure in the brief time they take to cross the bilayer, as a means of shielding their backbone polar groups from the nonpolar environment.

First we modeled TP2 on the membrane surface both as a helix and as an extended beta structure. Each was simulated for 3 ns and was found to bind stably. The average effective energy for the helical form was −239 kcal/mol and for the coil −231 kcal/mol. However, conformational entropy effects could easily compensate for the lower energy of the helix, giving a lower free energy for the extended structure (a rough estimate of Rln3 per torsion, for 24 torsions, gives ~16 kcal/mol favoring the coil). In addition, in simulations of unstructured peptides we identified a beta-hairpin structure with lower energy than the helix (see below). These results are consistent with the experimental observation of secondary structure with beta characteristics [75].

To study translocation, we first applied the same protocol as for the S4 helix. The peptides are constrained in a helical conformation and a regular grid of (z,θ) values is sampled. The resulting maps for TP2 and ONEG are shown in Fig. 7. TP2 has a broad global minimum at the interface with <W> about −239 kcal/mol. The transition state is at (0,0),

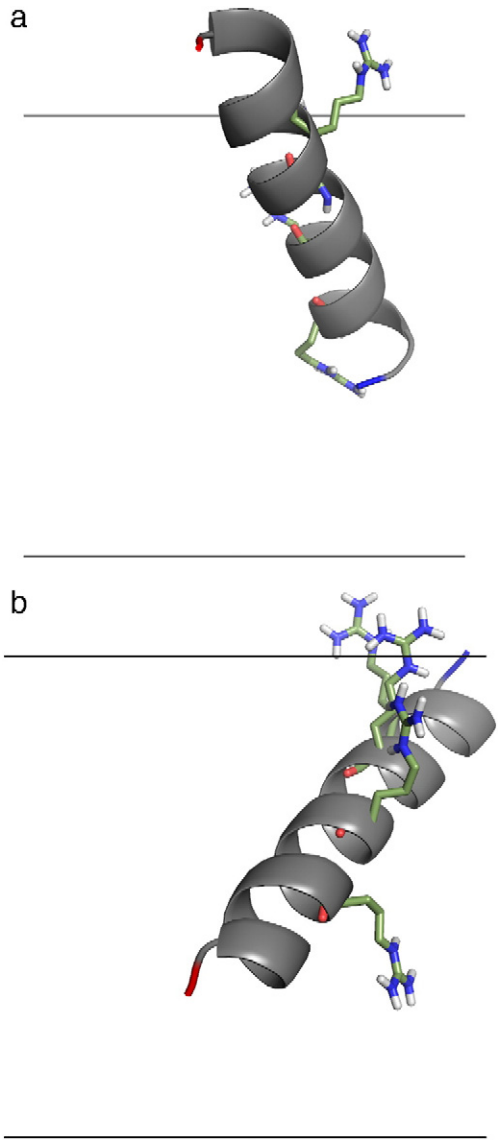

Fig. 6. Transition states for S4 translocation according to the map in Fig. 5. a) structure at z = 8 Å, θ = 40°, and b) structure at z = 5 Å, θ = 130°.

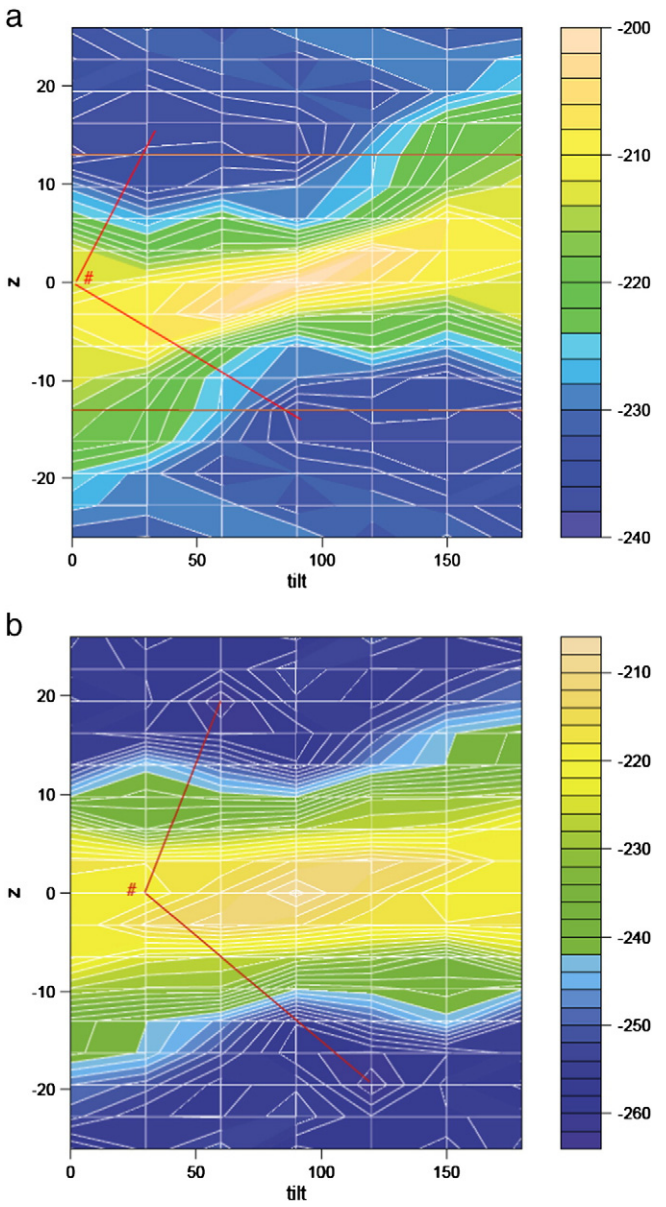

Fig. 7. Effective energy surface for a) TP2 and b) ONEG peptides in IMM1-LF. Symbols as in Fig. 5.

with <W> −214 kcal/mol, about 25 kcal/mol higher. ONEG does not have an interfacial minimum, consistent with its very weak binding [75]. Its TS is at (0,30) with a 44 kcal/mol barrier. It is satisfying that the negative control has a much higher barrier than the peptide that translocates.

Next we try to refine the transition state energy for the TP2 peptide by relaxing the assumption of a fully helical conformation and allowing membrane thinning. We perform simulations starting from the identified TS conformation at different membrane widths, releasing the helical constraints but maintaining the positional constraint for the center of mass. Table 4 shows the results. Releasing the helical constraints lowers the average effective energy to −219.1 kcal/mol. Thinning the membrane lowers the energy further. Adding the deformation energy we obtain an optimal value of about −223 kcal/mol.

Fig. 8a shows the structure of the TP2 peptide at the putative transition state. The helix is distorted and Gln 11 makes a hydrogen bond to the backbone. One Arg makes a salt bridge with the C-terminus and the other one a hydrogen bond with a backbone carbonyl. We checked whether neutralization of the termini at this configuration would reduce the free energy, but the result was negative.

In the results reported above the peptides were built as α-helices. We also performed simulations starting from unstructured TP2 peptide and constraining the center of mass at different z positions. These simulations identified a low energy beta hairpin structure at the interface (Fig. 8b) (<W> = −244.8 kcal/mol vs. −239 for the helix) but the average W at the membrane center was higher (−210.4 kcal/mol vs. −219.1 for the helix). If we accept the hairpin as the structure at the interface and the partial helix for the transition state, the barrier becomes ~22 kcal/mol.

3.7. Translocation of Wheaten–Almeida peptides

In recent work, Wheaten et al. used giant unilamellar vesicles to study the translocation of variants of transportan (TP10W), δ-lysin (DL1), and cecropin (CE2) and at the same time the dye leakage they cause when they interact with membranes [32]. They found that all peptides translocate, albeit to different extents, causing dye leakage. Interestingly, they found that TP10W can also translocate without leakage, suggesting that it can translocate directly through the membrane without forming a water pore.

We applied the same methodology as above to TP10W and DL1 (CE2 is very long as a single helix and probably requires a more complex treatment). The resulting map for TP10W with IMM1-LF is shown in Fig. 9. It exhibits a global minimum at the interface and a local minimum at the TM orientation, about 5 kcal/mol higher. The barriers correspond to crossing of the N and C termini and are about 15 kcal/mol higher than the global minimum. The same calculation for DL1 exhibits a barrier of ~30 kcal/mol. These results are consistent with the ability of the TP10W peptide to translocate even before dye leakage starts taking place [32]. Additional simulations at the interface (unconstrained) and at the (6,40) and (5.5,130) transition states (constrained) gave energies of −397 ± 2, −387 ± 2.0, and −388 ± 2 kcal/mol, respectively. The first barrier could be further lowered by N-terminus neutralization, but not the second (the C terminus is amidated). Thus, the refined estimate for the barrier is about 9 kcal/mol.

Table 4
Effective energy of the TS for TP2 translocation at different membrane thinning deformations.

	W	ΔG^{def}	$W + \Delta G^{def}$
T = 26	−219.1 ± 0.8	0	−219.1
T = 24	−221.1 ± 1.1	0.7	−220.4
T = 22	−224.3 ± 0.7	2.8	−221.5
T = 20	−228.7 ± 1.6	6.3	−222.4
T = 18	−234.3 ± 2.3	11.3	−223.0
T = 16	−232.8 ± 0.7	17.6	−215.2

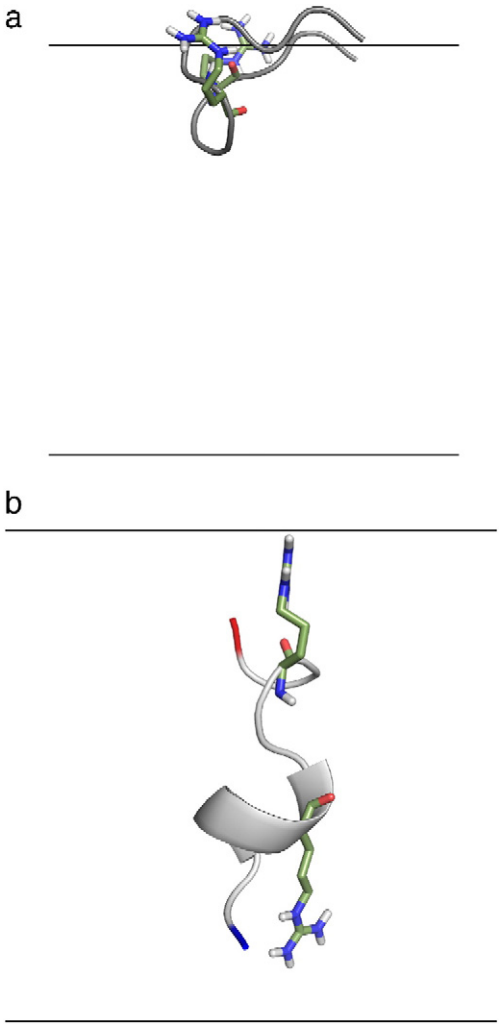

Fig. 8. Interfacial minimum (a) and putative transition state (b) for the TP2 peptide.

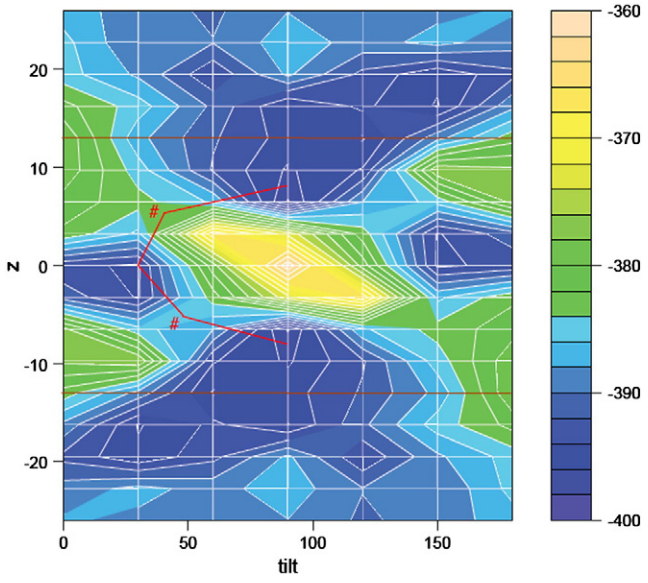

Fig. 9. Effective energy surface for the TP10W peptide in IMM1-LF. Symbols as in Fig. 5.

4. Discussion

Implicit membrane models [33,76–79] have obvious advantages but also significant drawbacks. Their computational efficiency allows rapid equilibration, extensive exploration of configurational space, and facile computation of free energy differences. The drawbacks include a severely simplified picture of a lipid bilayer, neglect of specific lipid–peptide interactions, neglect of the liquid-crystalline nature of the membrane interior and of the headgroup-acyl chain connectivity, and inability to deform. Here we show that some of these can be alleviated by incorporating data and insights from all-atom simulations and experiment. IMM1 is one model that has the versatility for this, since it is more empirical and is not tied to a particular theory, such as Poisson–Boltzmann or Generalized Born. Thus, the free energy profiles for different atom types can be individually modified. In this way, an implicit membrane model can serve as a summary of current physical knowledge. Expensive atomistic simulations can be used to obtain a fundamental quantity once, such as free energy profiles for functional groups, which are then incorporated into a simple model without the need to repeat the same calculation for different systems. This "hierarchical modeling" has a long history in computational chemistry (this is how force fields are derived from quantum chemical computations). It provides economy of effort and allows expansion of the range of problems that can be addressed. Such approaches provide a much faster way to test or formulate hypotheses for complex problems, which can then be tested by more detailed calculations.

Implicit membrane approaches face difficulties when the membrane deviates significantly from a hydrophobic slab. Although aqueous pores can be accounted for [80], other problems, such as aqueous crevices in membrane proteins, are more difficult to address. A second issue is the assumption of a homogeneous nonpolar membrane interior. This can be violated by charged groups, which have been observed to create water defects. Possible solutions to these problems have been explored in this work. For moderate thinning of the membrane, elasticity theory can provide estimates of the deformation cost. The water defects can be treated implicitly, by adopting the free energy profiles calculated in explicit simulations. This simple remedy has been found to improve things dramatically. However, it is not perfect. A water defect caused by a charged group will also affect the neighboring groups it comes in contact with. For example, it should lower somewhat the gain from the burial of hydrophobic groups that come in contact with it. These effects are neglected in the model presented here.

One area where implicit membrane models could prove useful is peptide translocation. Having a simplified energy function allows one to pursue more rigorous approaches for determining reaction pathways and transition states. The high cost of exposing the peptide backbone to the nonpolar membrane interior necessitates the formation of secondary structure and restricts the conformational space. Many peptides are likely to translocate as helices and this reduces the number of degrees of freedom that need to be considered. Here we used only two, which allows a visual determination of pathways and transition states. It should be noted, however, that such reduction in degrees of freedom can sometimes lead to missing the correct transition state, if the omitted degrees of freedom exhibit abrupt changes in neighboring points of the reduced surface [81,82]. This can be checked by examining the values of these omitted degrees of freedom, such as rotation angle and side chain conformations, and make sure they change smoothly along the putative minimum energy pathway. Computation of each of these energy maps takes about 5 h on a single processor. The TS identified in this way could serve as starting points for explicit simulations, such as umbrella sampling or transition path sampling simulations [83].

The membrane potential, which is negative in the cell interior, is known to play a key role in the translocation of cationic cell penetrating peptides [84]. It is not, however, present in most in vitro experiments. If desired, the membrane potential can easily be included in the calculations of the type presented here [85]. A positive membrane potential on the same side as the peptides will provide a driving force for translocation and will also lower the barriers. In that case symmetry will be lost and the calculation will have to be done in the entire range of z values. One could also include the effect of asymmetric membranes. For example, the presence of a neutral extracellular leaflet and a partially anionic intracellular leaflet could have impact on the translocation of cationic peptides.

Translating barrier heights to rate constants is not trivial, but rough estimates can be made. An exponential relationship is expected between the two, but the preexponential factor is uncertain. The classical TS theory formula, $kT/h\ \exp(-\Delta G^*/RT)$ uses as preexponential factor a fundamental quantum mechanical vibrational frequency ($kT/h = 6.2 \times 10^{12}\ s^{-1}$ at room temperature). This is usually regarded as an upper limit. In Kramers' theory [86], applicable to diffusional processes, the preexponential factor is $Dm\omega_b\omega_r/2\pi kT$, where D is the diffusion constant, m is the mass, and ω_b, ω_r are curvatures of the free energy profile at the barrier and the reactant wells. For a peptide in a lipid bilayer a value of about $10^{-7}\ cm^2/s$ has been calculated for D by MD simulations [87]. With this value and reasonable guesses for the curvatures, one arrives at the estimate $\sim 10^8\ s^{-1}$ for the preexponential factor. An alternative approach is the inhomogeneous solubility-diffusion model that has been mostly applied to small molecule permeants [88]. This approach gives the permeability as an integral of the free energy and the local diffusion constant along the membrane normal.

Using the classical TS formula and setting maximum observation time 1 day, the upper limit for a barrier is about 25 kcal/mol. With a $10^8\ s^{-1}$ preexponential factor, the upper limit is closer to 18 kcal/mol. This estimate seems reasonable, since a recent study of trp translocation found a time scale of 15 min to 4 h for a barrier of 17–18 kcal/mol [89]. The approximate barriers we calculated for the S4 helix (18.7 kcal/mol) and TP10W (9 kcal/mol) are close to or lower than this limit, and for TP2 slightly higher (22 kcal/mol). Of course, these are rough estimates which neglect, for example, interactions between titratable sites or configurational entropy contributions. For example, the rotation angle (which is not explicitly mapped) could have a narrow distribution at some points and a broad distribution at other points. From these preliminary results, the key for successful translocation without a pore seems to be a distribution of polar and charged groups that allows them to cross the membrane center at different points along the reaction coordinate. This way the barrier can be maintained at 10–20 kcal/mol.

It should be noted that in the experiments the peptides are modified by fluorescent dyes at the C-terminus [30,31] or the N-terminus [32]. Some of these dyes contain charges and are not able to permeate membranes by themselves. Questions arise then as to how the presence of the dyes affects the translocation of the peptides and vice versa, how the peptide facilitates the permeation of an otherwise impermeable dye. We will attempt to include these dyes in future modeling work.

On the basis of vesicle dye leakage experiments, Almeida and coworkers proposed that the free energy of insertion of the peptide into the membrane determines whether the peptide will translocate and the type of leakage [90]. Insertion free energies of less than 20 kcal/mol were proposed to allow peptide translocation and lead to graded leakage, whereas larger insertion free energies do not allow peptide translocation and lead to all-or-none leakage. More recent experiments showed this association to not be always valid [91,92]. The membrane insertion free energies were estimated by use of the water-to-octanol whole-residue hydrophobicity scale [93]. This approach has a number of shortcomings. First, octanol is not an ideal mimic of the membrane interior. Second, this approach ignores the effect of peptide configuration in the membrane and position of each residue in the sequence. Third, if peptide translocation occurs via pore formation, then membrane insertion free energies are not relevant. However, for peptide translocation through the membrane the idea is valid, provided that the true transition state structure is identified.

In an insightful paper, MacCallum and Tieleman [94] showed that the free energy of inserting two or three arginines in a membrane is much lower than one would expect from the free energy of inserting

one arginine. The mechanism for this is simple: most of the free energy cost of inserting an arginine involves the creation of a water defect. Once this cost is paid, inserting more arginines is relatively easy. Interestingly, when built as helices, the Marks–Wimley peptides place the arginines close to each other. Thus, they could "share" a water defect, lowering the cost of insertion. More fundamental studies of this nonadditivity are necessary, including detailed mapping of the free energy as a function of configuration of the arginines in the membrane. Nonadditivity of arginine insertion could be modeled as an effective attraction between them in the membrane interior that would be dependent on their distance and their position and orientation in the membrane. However, it did not appear essential in explaining the translocation ability of the peptides studied here.

Future work could include study of a larger number of peptides and negative controls, the effect of transmembrane voltage and membrane surface charge, the effect of different distributions of charge and polar groups, the difference between Lys and Arg, more extensive conformational search for the transition state, or development of automated procedures for titrating ionizable groups. Testing of the predictions by experiment is possible, for example, by designing sequence modifications that would increase or lower the translocation barriers.

Acknowledgments

This work was inspired by several talks at the ACS symposium "Interfacially active peptides", New Orleans, 2013 as well as a Telluride workshop on "Membrane Protein folding and Functioning", August 2013. Presentations and comments by W. Wimley, P. Almeida, and M. Berkowitz were especially helpful. Financial support by the National Science Foundation (MCB-1244207) is gratefully acknowledged. Infrastructure support was provided in part by RCMI grant 2G12RR03060-26A1/8G12MD007603-27 from NIH.

References

[1] A. Parsegian, Energy of an ion crossing a low dielectric membrane – solutions to 4 relevant electrostatic problems, Nature 221 (1969) 844-&.
[2] B.H. Honig, W.L. Hubbell, R.F. Flewelling, Electrostatic interactions in membranes and proteins, Annu. Rev. Biophys. Biophys. Chem. 15 (1986) 163–193.
[3] T. Hessa, S.H. White, G. von Heijne, Membrane insertion of a potassium-channel voltage sensor, Science 307 (2005) 1427-1427.
[4] C.P. Moon, K.G. Fleming, Side-chain hydrophobicity scale derived from transmembrane protein folding into lipid bilayers, Proc. Natl. Acad. Sci. U. S. A. 108 (2011) 10174–10177.
[5] M. Magzoub, A. Graslund, Cell-penetrating peptides: from inception to application, Q. Rev. Biophys. 37 (2004) 147–195.
[6] M.A. Wilson, A. Pohorille, Mechanism of unassisted ion transport across membrane bilayers, J. Am. Chem. Soc. 118 (1996) 6580–6587.
[7] J. Ulander, A.D.J. Haymet, Permeation across hydrated DPPC lipid bilayers: simulation of the titrable amphiphilic drug valproic acid, Biophys. J. 85 (2003) 3475–3484.
[8] A.C.V. Johansson, E. Lindahl, Amino-acid solvation structure in transmembrane helices from molecular dynamics simulations, Biophys. J. 91 (2006) 4450–4463.
[9] S. Dorairaj, T.W. Allen, On the thermodynamic stability of a charged arginine side chain in a transmembrane helix, Proc. Natl. Acad. Sci. U. S. A. 104 (2007) 4943–4948.
[10] J.L. MacCallum, W.F.D. Bennett, D.P. Tieleman, Partitioning of amino acid side chains into lipid bilayers: Results from computer simulations and comparison to experiment, J. Gen. Physiol. 129 (2007) 371–377.
[11] J.A. Freites, D.J. Tobias, G. von Heijne, S.H. White, Interface connections of a transmembrane voltage sensor, Proc. Natl. Acad. Sci. U. S. A. 102 (2005) 15059–15064.
[12] J.L. MacCallum, W.F.D. Bennett, D.P. Tieleman, Distribution of amino acids in a lipid bilayer from computer simulations, Biophys. J. 94 (2008) 3393–3404.
[13] T. Hessa, H. Kim, K. Bihlmaier, C. Lundin, J. Boekel, H. Andersson, I. Nilsson, S.H. White, G. von Heijne, Recognition of transmembrane helices by the endoplasmic reticulum translocon, Nature 433 (2005) 377–381.
[14] E.V. Schow, J.A. Freites, P. Cheng, A. Bernsel, G. von Heijne, S.H. White, D.J. Tobias, Arginine in membranes: the connection between molecular dynamics simulations and translocon-mediated insertion experiments, J. Membr. Biol. 239 (2011) 35–48.
[15] J. Gumbart, B. Roux, Determination of membrane-insertion free energies by molecular dynamics simulations, Biophys. J. 102 (2012) 795–801.
[16] A.C.V. Johansson, E. Lindahl, Protein contents in biological membranes can explain abnormal solvation of charged and polar residues, Proc. Natl. Acad. Sci. U. S. A. 106 (2009) 15684–15689.
[17] J. Gumbart, C. Chipot, K. Schulten, Free-energy cost for translocon-assisted insertion of membrane proteins, Proc. Natl. Acad. Sci. U. S. A. 108 (2011) 3596–3601.
[18] A. Rychkova, A. Warshel, Exploring the nature of the translocon-assisted protein insertion, Proc. Natl. Acad. Sci. U. S. A. 110 (2013) 495–500.
[19] K. Hristova, W.C. Wimley, A look at arginine in membranes, J. Membr. Biol. 239 (2011) 49–56.
[20] S. Choe, K.A. Hecht, M. Grabe, A continuum method for determining membrane protein insertion energies and the problem of charged residues, J. Gen. Physiol. 131 (2008) 563–573.
[21] K.M. Callenberg, N.R. Latorraca, M. Grabe, Membrane bending is critical for the stability of voltage sensor segments in the membrane, J. Gen. Physiol. 140 (2012) 55–68.
[22] A. Panahi, M. Feig, Dynamic Heterogeneous Dielectric Generalized Born (DHDGB): an implicit membrane model with a dynamically varying bilayer thickness, J. Chem. Theory Comput. 9 (2013) 1709–1719.
[23] N.J. Gleason, V.V. Vostrikov, D.V. Greathouse, R.E. Koeppe, Buried lysine, but not arginine, titrates and alters transmembrane helix tilt, Proc. Natl. Acad. Sci. U. S. A. 110 (2013) 1692–1695.
[24] J. Hoyer, I. Neundorf, Peptide vectors for the nonviral delivery of nucleic acids, Acc. Chem. Res. 45 (2012) 1048–1056.
[25] H.D. Herce, A.E. Garcia, Molecular dynamics simulations suggest a mechanism for translocation of the HIV-1 TAT peptide across lipid membranes, Proc. Natl. Acad. Sci. U. S. A. 104 (2007) 20805–20810.
[26] S. Yesylevskyy, S.J. Marrink, A.E. Mark, Alternative mechanisms for the interaction of the cell-penetrating peptides penetratin and the TAT peptide with lipid bilayers, Biophys. J. 97 (2009) 40–49.
[27] K. Huang, A.E. Garcia, Free energy of translocating an arginine-rich cell-penetrating peptide across a lipid bilayer suggests pore formation, Biophys. J. 104 (2013) 412–420.
[28] M. Pourmousa, J. Wong-ekkabut, M. Patra, M. Karttunen, Molecular dynamic studies of transportan interacting with a DPPC lipid bilayer, J. Phys. Chem. B 117 (2013) 230–241.
[29] K. Matsuzaki, O. Murase, N. Fujii, K. Miyajima, Translocation of a channel-forming antimicrobial peptide, magainin 2, across lipid bilayers by forming a pore, Biochemistry 34 (1995) 6521–6526.
[30] J.R. Marks, J. Placone, K. Hristova, W.C. Wimley, Spontaneous membrane-translocating peptides by orthogonal high-throughput screening, J. Am. Chem. Soc. 133 (2011) 8995–9004.
[31] J. He, K. Hristova, W.C. Wimley, A highly charged voltage-sensor helix spontaneously translocates across membranes, Angew. Chem. Int. Ed. 51 (2012) 7150–7153.
[32] A.A. Wheaten, F.D.O. Ablan, B.L. Spaller, J.M. Trieu, P.F. Almeida, Translocation of cationic amphipathic peptides across the membrane of pure phospholipid giant vesicles, J. Am. Chem. Soc. 135 (2013) 16517–16525.
[33] T. Lazaridis, Effective energy function for proteins in lipid membranes, Proteins Struct. Funct. Genet. 52 (2003) 176–192.
[34] T. Lazaridis, M. Karplus, Effective energy function for proteins in solution, Proteins 35 (1999) 133–152.
[35] E. Neria, S. Fischer, M. Karplus, Simulation of activation free energies in molecular systems, J. Chem. Phys. 105 (1996) 1902–1921.
[36] T. Lazaridis, Implicit solvent simulations of peptide interactions with anionic lipid membranes, Proteins 58 (2005) 518–527.
[37] L.B. Li, I. Vorobyov, T.W. Allen, Potential of mean force and pK(a) profile calculation for a lipid membrane-exposed arginine side chain, J. Phys. Chem. B 112 (2008) 9574–9587.
[38] A.C.V. Johansson, E. Lindahl, Titratable amino acid solvation in lipid membranes as a function of protonation state, J. Phys. Chem. B 113 (2009) 245–253.
[39] L.B.B. Li, I. Vorobyov, T.W. Allen, The role of membrane thickness in charged protein–lipid interactions, Biochim. Biophys. Acta Biomembr. 1818 (2012) 135–145.
[40] A. Kessel, D.P. Tieleman, N. Ben-Tal, Implicit solvent model estimates of the stability of model structures of the alamethicin channel, Eur. Biophys. J. 33 (2004) 16–28.
[41] L. Prieto, T. Lazaridis, Computational studies of colicin insertion into membranes: the closed state, Proteins 79 (2011) 126–141.
[42] C. Nielsen, M. Goulian, O.S. Andersen, Energetics of inclusion-induced bilayer deformations, Biophys. J. 74 (1998) 1966–1983.
[43] J.A. Lundbaek, O.S. Andersen, Spring constants for channel-induced lipid bilayer deformations estimates using gramicidin channels, Biophys. J. 76 (1999) 889–895.
[44] Y.H. Kao, C.A. Fitch, S. Bhattacharya, C.J. Sarkisian, J.T.J. Lecomte, B. Garcia-Moreno, Salt effects on ionization equilibria of histidines in myoglobin, Biophys. J. 79 (2000) 1637–1654.
[45] J.P. Ryckaert, G. Ciccotti, H.J.C. Berendsen, Numerical-integration of Cartesian equations of motion of a system with constraints — molecular-dynamics of N-alkanes, J. Comput. Phys. 23 (1977) 327–341.
[46] J.Y. Lee, W.P. Im, Restraint potential and free energy decomposition formalism for helical tilting, Chem. Phys. Lett. 441 (2007) 132–135.
[47] R. Core Team, R: A language and environment for statistical computing, R Foundation for Statistical Computing, Vienna, Austria, 2013. URL http://www.R-project.org/.
[48] A. Masunov, T. Lazaridis, Potentials of mean force between ionizable amino acid sidechains in aqueous solution, J. Am. Chem. Soc. 125 (2003) 1722–1730.
[49] J.L. Maccallum, D.P. Tieleman, Calculation of the water-cyclohexane transfer free energies of neutral amino acid side-chain analogs using the OPLS all-atom force field, J. Comput. Chem. 24 (2003) 1930–1935.
[50] C. Neale, W.F.D. Bennett, D.P. Tieleman, R. Pomes, Statistical convergence of equilibrium properties in simulations of molecular solutes embedded in lipid bilayers, J. Chem. Theory Comput. 7 (2011) 4175–4188.
[51] A. Radzicka, R. Wolfenden, Comparing the polarities of the amino acids: side-chain distribution coefficients between the vapor hase, cyclohexane, 1-octanol, and neutral aqueous solution, Biochemistry 27 (1988) 1664–1670.

[52] L.B. Li, I. Vorobyov, T.W. Allen, The different interactions of lysine and arginine side chains with lipid membranes, J. Phys. Chem. B 117 (2013) 11906–11920.
[53] C. Chipot, A. Pohorille, Folding and translocation of the undecamer of poly-L-leucine across the water-hexane interface. A molecular dynamics study, J. Am. Chem. Soc. 120 (1998) 11912–11924.
[54] L. Li, I. Vorobyov, A.D. MacKerell, T.W. Allen, Is arginine charged in a membrane? Biophys. J. 94 (2008) L11–L13.
[55] J. Yoo, Q. Cui, Does arginine remain protonated in the lipid membrane? Insights from microscopic pK(a) calculations, Biophys. J. 94 (2008) L61–L63.
[56] J. Yoo, Q.A. Cui, Chemical versus mechanical perturbations on the protonation state of arginine in complex lipid membranes: insights from microscopic pK(a) calculations, Biophys. J. 99 (2010) 1529–1538.
[57] D.G. Isom, C.A. Castaneda, B.R. Cannon, B.E. Garcia-Moreno, Large shifts in pK(a) values of lysine residues buried inside a protein, Proc. Natl. Acad. Sci. U. S. A. 108 (2011) 5260–5265.
[58] Y.X. Jiang, A. Lee, J.Y. Chen, V. Ruta, M. Cadene, B.T. Chait, R. MacKinnon, X-ray structure of a voltage-dependent K+ channel, Nature 423 (2003) 33–41.
[59] S.Y. Lee, A. Lee, J.Y. Chen, R. MacKinnon, Structure of the KvAP voltage-dependent K+ channel and its dependence on the lipid membrane, Proc. Natl. Acad. Sci. U. S. A. 102 (2005) 15441–15446.
[60] S.B. Long, E.B. Campbell, R. MacKinnon, Crystal structure of a mammalian voltage-dependent Shaker family K+ channel, Science 309 (2005) 897–903.
[61] S.B. Long, X. Tao, E.B. Campbell, R. MacKinnon, Atomic structure of a voltage-dependent K+ channel in a lipid membrane-like environment, Nature 450 (2007) 376-U373.
[62] L.G. Cuello, D.M. Cortes, E. Perozo, Molecular architecture of the KvAP voltage-dependent K+ channel in a lipid bilayer, Science 306 (2004) 491–495.
[63] D. Krepkiy, M. Mihailescu, J.A. Freites, E.V. Schow, D.L. Worcester, K. Gawrisch, D.J. Tobias, S.H. White, K.J. Swartz, Structure and hydration of membranes embedded with voltage-sensing domains, Nature 462 (2009) 473-U168.
[64] J.A. Freites, D.J. Tobias, S.H. White, A voltage-sensor water pore, Biophys. J. 91 (2006) L90–L92.
[65] W. Treptow, M. Tarek, Environment of the gating charges in the Kv1.2 Shaker potassium channel, Biophys. J. 90 (2006) L64–L66.
[66] V. Jogini, B. Roux, Dynamics of the Kv1.2 voltage-gated K(+) channel in a membrane environment, Biophys. J. 93 (2007) 3070–3082.
[67] Z.A. Sands, M.S.P. Sansom, How does a voltage sensor interact with a lipid bilayer? Simulations of a potassium channel domain, Structure 15 (2007) 235–244.
[68] P.J. Bond, M.S.P. Sansom, Bilayer deformation by the Kv channel voltage sensor domain revealed by self-assembly simulations, Proc. Natl. Acad. Sci. U. S. A. 104 (2007) 2631–2636.
[69] T. Doherty, Y.C. Su, M. Hong, High-resolution orientation and depth of insertion of the voltage-sensing S4 helix of a potassium channel in lipid bilayers, J. Mol. Biol. 401 (2010) 642–652.
[70] C.L. Wee, A. Chetwynd, M.S.P. Sansom, Membrane insertion of a voltage sensor helix, Biophys. J. 100 (2011) 410–419.
[71] M. Fernandez-Vidal, F. Castro-Roman, S.H. White, Membrane insertion of a S4 potassium channel voltage sensor: an experimental study, Biophys. J. 90 (2006) 1164.
[72] H. PeledZehavi, I.T. Arkin, D.M. Engelman, Y. Shai, Coassembly of synthetic segments of shaker K+ channel within phospholipid membranes, Biochemistry 35 (1996) 6828–6838.
[73] A. Halsall, C.E. Dempsey, Intrinsic helical propensities and stable secondary structure in a membrane-bound fragment (S4) of the Shaker potassium channel, J. Mol. Biol. 293 (1999) 901–915.
[74] R. Brasseur, G. Divita, Happy birthday cell penetrating peptides: already 20 years, Biochim. Biophys. Acta Biomembr. 1798 (2010) 2177–2181.
[75] J. Cruz, M. Mihailescu, G. Wiedman, K. Herman, P.C. Searson, W.C. Wimley, K. Hristova, A membrane-translocating peptide penetrates into bilayers without significant bilayer perturbations, Biophys. J. 104 (2013) 2419–2428.
[76] V.Z. Spassov, L. Yan, S. Szalma, Introducing an implicit membrane in generalized born/solvent accessibility continuum solvent models, J. Phys. Chem. B 106 (2002) 8726–8738.
[77] W. Im, M. Feig, C.L. Brooks III, An implicit membrane GB theory for the study of structure, stability, and interactions of membrane proteins, Biophys. J. 85 (2003) 2900–2918.
[78] S. Tanizaki, M. Feig, A generalized Born formalism for heterogeneous dielectric environments: application to the implicit modeling of biological membranes, J. Chem. Phys. 122 (2005).
[79] M.B. Ulmschneider, J.P. Ulmschneider, M.S.P. Sansom, A. Di Nola, A generalized Born implicit-membrane representation compared to experimental insertion free energies, Biophys. J. 92 (2007) 2338–2349.
[80] T. Lazaridis, Structural determinants of transmembrane beta-barrels, J. Chem. Theory Comput. 1 (2005) 716–722.
[81] T. Lazaridis, D.J. Tobias, C.L. Brooks, M.E. Paulaitis, Reaction paths and free-energy profiles for conformational transitions — an internal coordinate approach, J. Chem. Phys. 95 (1991) 7612–7625.
[82] T. Lazaridis, M.E. Paulaitis, Computational study of conformational transitions in the active-site of tosyl-alpha-chymotrypsin, J. Am. Chem. Soc. 116 (1994) 1546–1556.
[83] P.G. Bolhuis, D. Chandler, C. Dellago, P.L. Geissler, Transition path sampling: throwing ropes over rough mountain passes, in the dark, Annu. Rev. Phys. Chem. 53 (2002) 291–318.
[84] D. Terrone, S.L.W. Sang, L. Roudaia, J.R. Silvius, Penetratin and related cell-penetrating cationic peptides can translocate across lipid bilayers in the presence of a transbilayer potential, Biochemistry 42 (2003) 13787–13799.
[85] M. Mottamal, T. Lazaridis, Voltage-dependent energetics of alamethicin monomers in the membrane, Biophys. Chem. 122 (2006) 50–57.
[86] H.A. Kramers, Brownian motion in a field of force and the diffusion model of chemical reactions, Physica 7 (1940) 284–304.
[87] V. Vivcharuk, Y.N. Kaznessis, Thermodynamic analysis of protegrin-1 insertion and permeation through a lipid bilayer, J. Phys. Chem. B 115 (2011) 14704–14712.
[88] S.J. Marrink, H.J.C. Berendsen, Simulation of water transport through a lipid-membrane, J. Phys. Chem. 98 (1994) 4155–4168.
[89] A.E. Cardenas, G.S. Jas, K.Y. DeLeon, W.A. Hegefeld, K. Kuczera, R. Elber, Unassisted transport of N-acetyl-L-tryptophanamide through membrane: experiment and simulation of kinetics, J. Phys. Chem. B 116 (2012) 2739–2750.
[90] P.F. Almeida, A. Pokorny, Mechanisms of antimicrobial, cytolytic, and cell-penetrating peptides: from kinetics to thermodynamics, Biochemistry 48 (2009) 8083–8093.
[91] K.S. Clark, J. Svetlovics, A.N. McKeown, L. Huskins, P.F. Almeida, What determines the activity of antimicrobial and cytolytic peptides in model membranes, Biochemistry 50 (2011) 7919–7932.
[92] S.A. Wheaten, A. Lakshmanan, P.F. Almeida, Statistical analysis of peptide-induced graded and all-or-none fluxes in giant vesicles, Biophys. J. 105 (2013) 432–443.
[93] S.H. White, W.C. Wimley, Membrane protein folding and stability: physical principles, Annu. Rev. Biophys. Biomol. Struct. 28 (1999) 319–365.
[94] J.L. MacCallum, W.F.D. Bennett, D.P. Tieleman, Transfer of arginine into lipid bilayers is nonadditive, Biophys. J. 101 (2011) 110–117.